Journal of Power Sources 192 (2009) 467–474

Contents lists available at ScienceDirect

Journal of Power Sources

journal homepage: www.elsevier.com/locate/jpowsour

On modeling multi-component diffusion inside the porous anode of solid oxide fuel cells using Fick's model

Fatma N. Cayan*, Suryanarayana R. Pakalapati, Francisco Elizalde-Blancas, Ismail Celik

Department of Mechanical and Aerospace Engineering, West Virginia University, P.O. Box 6106, Morgantown, WV, USA

ARTICLE INFO

Article history:
Received 28 January 2009
Received in revised form 10 March 2009
Accepted 11 March 2009
Available online 24 March 2009

Keywords:
Solid oxide fuel cells
Multi-component diffusion
Effective diffusivity
Coal syngas
Modeling

ABSTRACT

Stefan–Maxwell model (SMM) and simple Fick's model (FM) type of relations both including Knudsen diffusion for the calculation of species mole fraction distribution inside the porous anode of a solid oxide fuel cell (SOFC) were compared and it was found that at low current densities the models agree well but as current increases the differences also increase. Based on the findings an empirical correction is proposed for the effective diffusivity used in Fick's model. The corrected diffusivity coefficient gave better agreement with the Stefan–Maxwell model and even at higher current densities the error is less than 5%. This correction was implemented via a three-dimensional, in-house SOFC simulation code (DREAMSOFC) which uses Fick's model type relations for diffusion flux calculations. The code also takes into account methane steam reforming (MSR) and water gas shift (WGS) reactions and the electrochemical oxidation of both H_2 and CO. As an application, a SOFC button cell which is being tested at West Virginia University was simulated. The results with and without the proposed correction for effective diffusivity are compared.

1. Introduction

Solid oxide fuel cells (SOFCs) are perceived to be the most viable candidates for future power plants due to their high efficiency and fuel flexibility. The performance of a SOFC at high operating current densities is reduced mainly due to the mass transport losses, that is, the demand for reactants exceeds their capacity to diffuse through the porous anode to the reaction site at the anode–electrolyte interface. The multi-component mass transport in SOFC anodes is also coupled with the bulk chemical reactions and the resulting diffusion and reaction time scales of different species dictate the limiting behavior. Accurate modeling of this phenomenon is imperative for development of better fuel cell designs.

The equations governing the multi-component mass transfer include Stefan–Maxwell relations for calculation of specie fluxes. These relations are coupled, nonlinear system of partial differential equations and are cumbersome to solve, especially when a large number of species are involved as in the case of coal syngas. Alternatively, simple Fick's law type relations with an effective multi-component diffusivity, which can be directly substituted into the specie conservation equation, are generally used to model the diffusion fluxes [1–4]. However, the validity of such simplified models is not well established. Suwanwarangkul et al. [5], for example, compared these two approaches for a simple one-dimensional case without bulk chemical reactions and recommended the use of Stefan–Maxwell relations including the effect of Knudsen diffusion for multi-component systems. However, several authors [6–8] predicted the limiting behavior of the experimental VI curves using Fick's law type relations for the diffusion fluxes. In such studies, tortuosity values as high as 14.5 were used during calibration [6] whereas some studies show that the actual tortuosities for porous electrodes are in the range of 2–6 [9,10]. Thus, it is necessary to look for other factors that may affect the effective multi-component diffusion coefficients used in Fick's law type relations rather than using unphysically high tortuosity values.

In this paper, we compare these two approaches by simulating mass transfer inside an SOFC anode operating on coal syngas consisting of CH_4, H_2, CO, H_2O, CO_2 and N_2. A two-dimensional computer code was developed for the solution of models based on Stefan–Maxwell and Fick's law flux relations to predict the specie concentration distribution inside the porous anode. Methane steam reforming and water gas shift reactions are taken into account in addition to the electrochemical reactions at the anode/electrolyte interface and chemical kinetics modeling was employed for the bulk reactions. The ratio between the current produced by CO and H_2 oxidation is assumed to be constant. Comparisons show that at low current densities the models agree well but as current increases the differences increase. The error in the Fick's law model was positive for the reactants and negative for the products. Based on these findings an empirical correction is proposed for the effective diffusivity used in Fick's model. Model parameters were found by calibrating it with the Stefan–Maxwell model using the two-dimensional code.

* Corresponding author. Tel.: +1 304 293 3111; fax: +1 304 293 6689.
E-mail address: fcayan@mix.wvu.edu (F.N. Cayan).

0378-7753/$ – see front matter © 2009 Elsevier B.V. All rights reserved.
doi:10.1016/j.jpowsour.2009.03.026

Nomenclature

c	model parameter
D_i^{eff}	effective diffusivity ($m^2\ s^{-1}$)
D_i^{eff*}	corrected effective diffusivity ($m^2\ s^{-1}$)
D_i^k	Knudsen diffusivity ($m^2\ s^{-1}$)
D_{ij}	binary diffusivity ($m^2\ s^{-1}$)
D_i^{k*}	effective Knudsen diffusivity ($m^2\ s^{-1}$)
D_{ij}^*	effective binary diffusivity ($m^2\ s^{-1}$)
i	total current density ($A\ m^{-2}$)
i_{ref}	reference current density ($A\ m^{-2}$)
k_r^+	forward reaction rate constant for methane steam reforming reaction ($mol\ m^{-3}\ s^{-1}\ Pa^{-2}$)
k_r^-	backward reaction rate constant for methane steam reforming reaction ($mol\ m^{-3}\ s^{-1}\ Pa^{-4}$)
k_s^+, k_s^-	forward and backward reaction rate constants for water gas shift reaction ($mol\ m^{-3}\ s^{-1}\ Pa^{-2}$)
M_i	molecular weight of species *i* ($g\ mol^{-1}$)
M_{avg}	average molecular weight ($g\ mol^{-1}$)
n	model parameter
N_i	molar flux ($mol\ m^{-2}\ s^{-1}$)
P	pressure of the system (Pa)
R	universal gas constant ($J\ mol^{-1}\ K^{-1}$)
R_i	molar production rate of species *i* ($mol\ m^{-3}\ s^{-1}$)
$\langle r \rangle$	mean pore radius (μm)
T	temperature of the system (K)
y_i	mole fractions
ε	porosity
ν_i	stoichiometric coefficient
τ	tortuosity

Proposed correction for effective diffusivity was then applied to a three-dimensional, in-house SOFC simulation code (DREAM-SOFC) which uses Fick's law type relations for diffusion flux calculations. As an application, an SOFC button cell which is being tested at West Virginia University was simulated. The results with and without the proposed correction for effective diffusivity were compared.

2. Description of the method

Diffusion transport inside the porous medium has two components: bulk molecular diffusion where molecular to molecular interaction dominates the transport and Knudsen diffusion where molecular to solid wall interaction dominates the transport. Several different approaches have been developed to evaluate multi-component porous media transport [3,11,12]. In the present study, Stefan–Maxwell model (SMM) and Fick's model (FM) both of which include the effect of Knudsen diffusion in addition the bulk molecular diffusion were used.

The flux expression in Stefan–Maxwell model is given by [13]

$$\frac{N_i}{D_i^{k*}} + \sum_{\substack{j=1 \\ j\neq i}}^{n} \frac{y_j N_i - y_i N_j}{D_{ij}^*} = -\frac{P}{RT}\nabla y_i \tag{1}$$

where N_i and y_i are the molar fluxes and mole fractions of species, D_{ij}^* and D_i^{k*} are effective binary and Knudsen diffusivities. The first term on the left hand side accounts for the Knudsen diffusion and the second one signifies the multi-component bulk molecular diffusion.

The effective binary diffusivity is usually defined as:

$$D_{ij}^* = \frac{\varepsilon}{\tau} D_{ij} \tag{2}$$

where ε and τ are the bulk porosity and tortuosity, respectively. D_{ij} is the binary diffusivity and can be calculated using Chapman–Enskog relations [13]:

$$D_{ij} = 0.001858 \frac{[T^3(M_i + M_j)/M_i M_j]^{1/2}}{P\sigma_{ij}^2 \Omega_D} \tag{3}$$

where T and P are the temperature and the pressure of the system, respectively. M_i represents the molecular weight of species *i*. σ_{ij} is given by

$$\sigma_{ij} = \frac{\sigma_i + \sigma_j}{2} \tag{4}$$

σ_i is the collision diameter of species *i*. The dimensionless parameter Ω_D is the collision integral calculated as:

$$\Omega_D = \frac{A}{T_N^B} + \frac{C}{\exp(DT_N)} + \frac{E}{\exp(FT_N)} + \frac{G}{\exp(HT_N)} \tag{5}$$

where the coefficients *A*, *B*, *C*, *D*, *E*, *F*, *G*, *H* are 1.06036, 0.1561, 0.193, 0.47635, 1.03587, 1.52996, 1.76474, 3.89411, respectively [14]. The dimensionless temperature T_N is defined as:

$$T_N = \frac{kT}{\varepsilon_{ij}} \tag{6}$$

where k is the Boltzmann constant. The term ε_{ij} is calculated as:

$$\varepsilon_{ij} = (\varepsilon_i \varepsilon_j)^{1/2} \tag{7}$$

where ε_i is the characteristic Lennard–Jones energy of species *i*.

Likewise Knudsen diffusivity is defined as:

$$D_i^{k*} = \frac{\varepsilon}{\tau} \langle r \rangle \frac{2}{3} \sqrt{\frac{8RT}{\pi M_i}} \tag{8}$$

where $\langle r \rangle$ is the mean pore radius, R is the universal gas constant and M_i is the molecular weight of the species *i*.

Fick's model (FM), simplest form used to describe the transport of species in the gas phase, is defined as:

$$N_i = -D_i^{eff} \frac{P}{RT} \nabla y_i \tag{9}$$

where D_i^{eff} is the effective diffusivity. Simulations with Fick's model were conducted by using the effective diffusivity proposed by Yakabe et al. [3]:

$$D_i^{eff} = \frac{\varepsilon}{\tau} \left[\frac{1 - \alpha_{i,m} y_i}{D_{i,m}} + \frac{1}{D_i^k} \right]^{-1} \tag{10}$$

$\alpha_{i,m}$ is a dimensionless parameter given by

$$\alpha_{i,m} = 1 - \left(\frac{M_i}{M_{avg}} \right)^{1/2} \tag{11}$$

where M_{avg} is the average molecular weight of the mixture and M_i is the molecular weight of the species *i*. Multi-component molecular diffusivity of species *i* in the mixture D_{im} is given by

$$D_{i,m} = \frac{1 - y_i}{\sum_{j \neq i} \frac{y_j}{D_{ij}}} \tag{12}$$

The calculated molar fluxes either from SMM (Eq. (1)) or from FM (Eq. (9)) are then used to determine the rate of change of specie concentrations through the following conservation equation:

$$\varepsilon \frac{P}{RT} \frac{\partial y_i}{\partial t} = -\nabla N_i + R_i \tag{13}$$

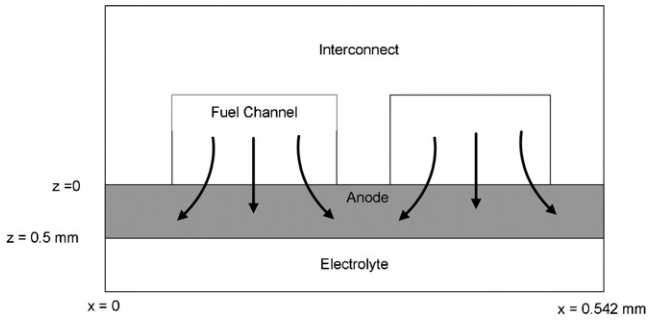

Fig. 1. Schematic representation of components of a solid oxide fuel cell.

where R_i is the molar rate of production of species i due to bulk chemical reactions.

In the present study, the principle bulk chemical reactions of concern are methane steam reforming and water gas shift reactions, described respectively as:

$$CH_4 + H_2O \underset{k_r^-}{\overset{k_r^+}{\rightleftharpoons}} 3H_2 + CO \tag{14}$$

$$CO + H_2O \underset{k_s^-}{\overset{k_s^+}{\rightleftharpoons}} CO_2 + H_2 \tag{15}$$

where k_r^+ and k_r^- are the forward and backward reaction rate constants for reforming reaction and k_s^+ and k_s^- are the reaction rate constants for shift reaction. Experimentally determined values for these rate constants and their Arrhenius form can be found in [15,16]. The net reaction rates are given for reforming and shift reactions, respectively as:

$$R_r = k_r^+ p_{CH_4} p_{H_2O} - k_r^- p_{CO} (p_{H_2})^3 \tag{16}$$

$$R_s = k_s^+ p_{CO} p_{H_2O} - k_s^- p_{CO_2} p_{H_2} \tag{17}$$

The specified boundary conditions are the specie concentration at the anode fuel channel interface and molar fluxes at anode–electrolyte interface proportional to the prescribed cell current. It was assumed that there is zero flux for other boundaries. The ratio between the current produced by CO and H_2 oxidation is assumed to be constant and taken as 4 for the current study [17].

3. Results and discussions

As explained in the previous section SMM and FM are two of the models which are used to calculate the fluxes of each species in a multi-component system. In this paper, these two approaches were compared by simulating mass transfer inside an SOFC anode operating on coal syngas consisting of CH_4, H_2, CO, H_2O, CO_2 and N_2 (see Table 3). A schematic representation of the SOFC anode which is used for simulation is shown in Fig. 1. A two-dimensional computer code was developed for the solution of models based on Stefan–Maxwell and Fick's law flux relations to predict the specie concentration distribution inside the porous anode.

The predictive ability of the developed code is verified by comparing the results of molar formation rates to those of [15] that also used SMM to predict the species molar fluxes. Fig. 2 shows a good agreement between two independent calculations which indicates the model was successfully implemented.

In what follows, the 2D code validated above is used to compare the results obtained using Fick's model for diffusion flux with those obtained using Stefan–Maxwell model. Fig. 3 shows the maximum

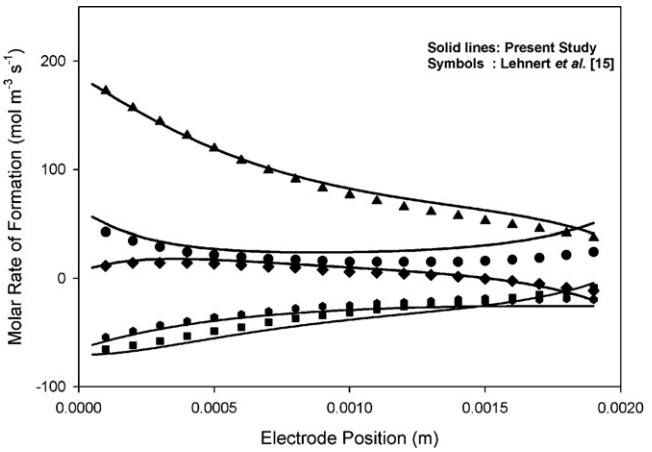

Fig. 2. Comparison between the molar rate of formation results of the present study and those of [15].

percentage error (deviation from SMM predictions of concentration) of Fick's model versus current density.

As can be seen from the figure, at low current densities the models agree well but as current increases the differences increase to up to 20% at a current density of 4 A cm^{-2}. The error in the Fick's law model is positive for the fuel species (reactants) and negative for the products. Based on these findings an empirical correction is

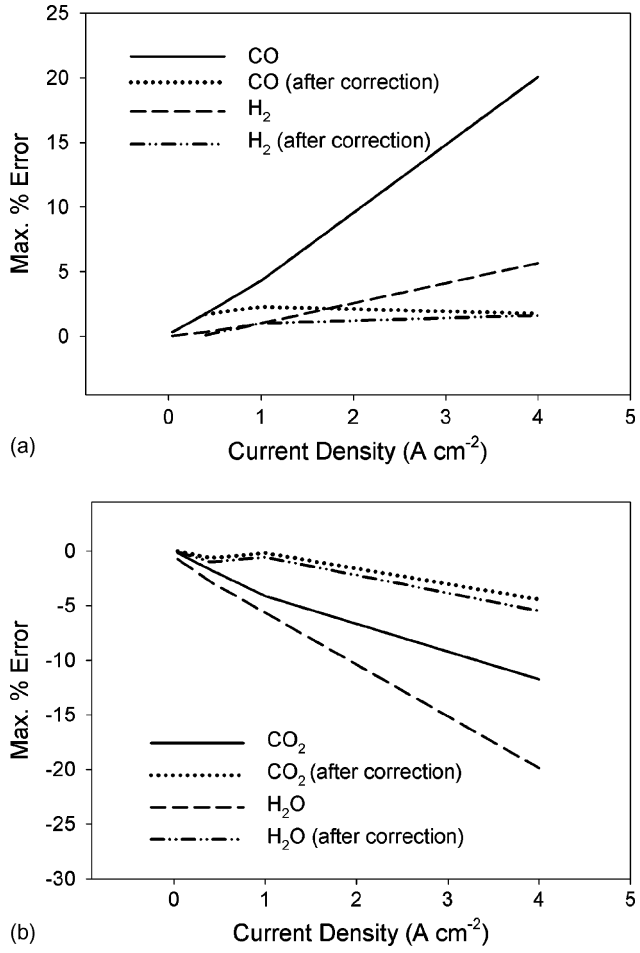

Fig. 3. Maximum percentage error of Fick's model versus current density for (a) reactants, (b) products.

Table 1
Coal syngas composition.

Species	Mole fractions
CO	0.291
H_2	0.285
CO_2	0.118
H_2O	0.276
CH_4	0.021
N_2	0.009

Table 2
Anode properties.

	Value
Thickness (mm)	0.5
Width (mm)	0.542
Tortuosity	3.6
Porosity	0.56
Mean pore diameter, $\langle r \rangle$ (μm)	1.07
Operating temperature (K)	1123

proposed for the effective diffusivity used in Fick's law model as:

$$D_i^{eff*} = D_i^{eff}\left(1 + sign(\nu_i)c\frac{i}{i_{ref}}\right)^n \quad (18)$$

where ν_i is the stoichiometric coefficient, i is the total current density and i_{ref} is the reference current density taken as 1 A m^{-2}. Model parameters c and n are found as 4.88×10^{-4} and 2, respectively, by calibrating it with the SMM using the two-dimensional code presented here.

The corrected diffusivities were used to predict the species concentration distribution inside an SOFC anode running on coal syngas. Anode was treated as a two-dimensional medium. Tables 1 and 2 show the syngas composition and the anode electrode properties used for simulations.

Mole fraction distributions inside the porous anode directly below the fuel channel is given in Figs. 4 and 5 for operating current densities of 1 A cm^{-2} and 4 A cm^{-2}, respectively. As can be seen from the figures the corrected diffusivity coefficient gave better agreement with the Stefan–Maxwell model and even at higher current densities the error is less than 5% (see Fig. 3). Since this correction is based on numerical experiments it is expected to have some errors and 5% error is acceptable for such a heuristic model.

Table 3
Normalized diffusion time scales.

Species	τ_{diff}/τ_{conv}
CO	0.030486
H_2	0.008841
CO_2	0.038900
H_2O	0.025321
CH_4	0.028375

The estimated reaction and diffusion time scales for the conditions used in the above simulation normalized with the flow through time ($\tau_{conv} = L/u = 0.267$ s with L being fuel channel length and u being average velocity inside the channel) of the fuel in the gas channel are given in Tables 3 and 4 respectively. It can be seen from Table 3 that there is ample time for the component species to diffuse through the anode as they flow through the gas channel.

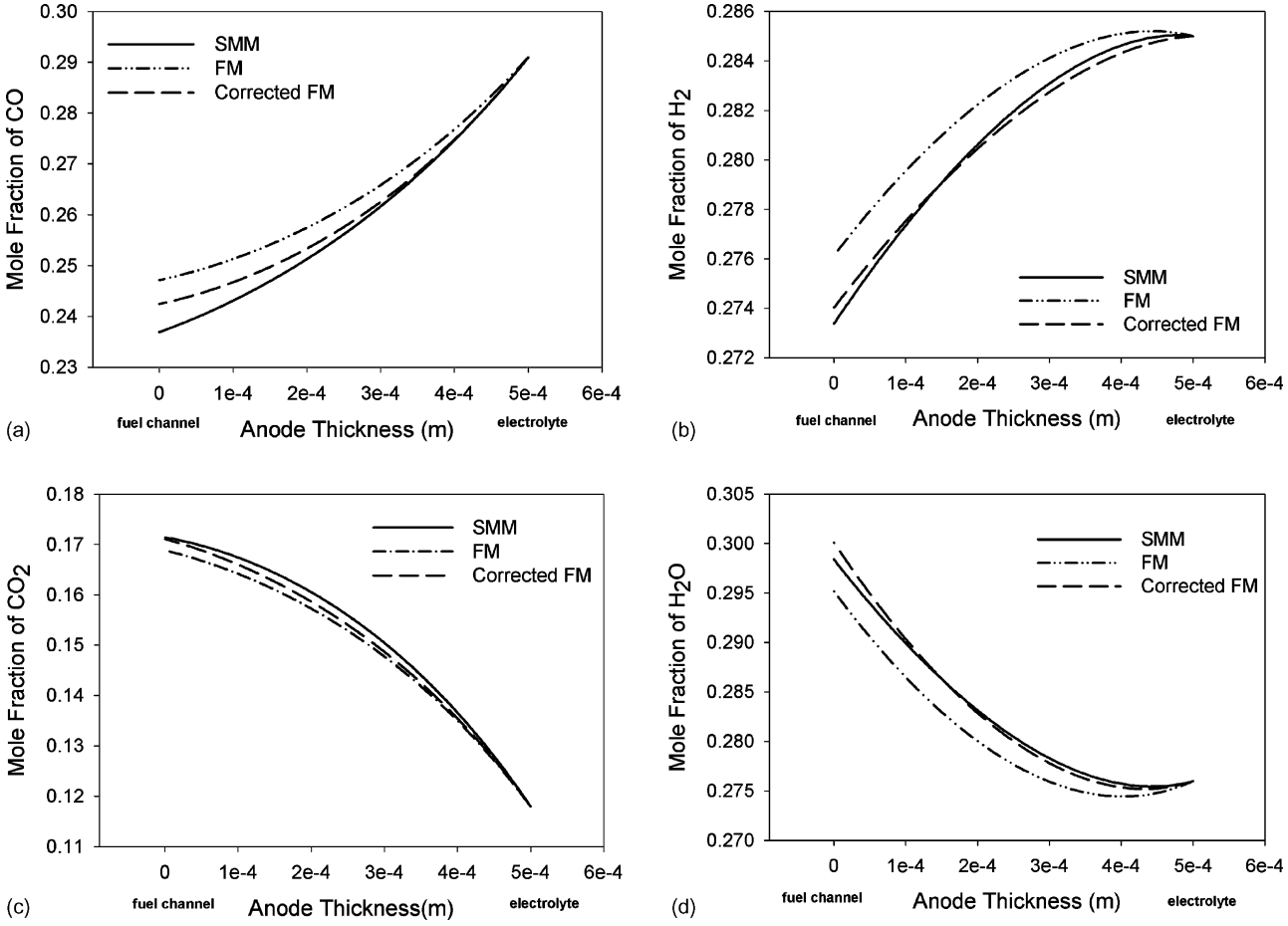

Fig. 4. Concentration profiles along the anode thickness predicted by FM and SMM for (a) CO, (b) H_2, (c) CO_2 and (d) H_2O at 1 A cm^{-2}.

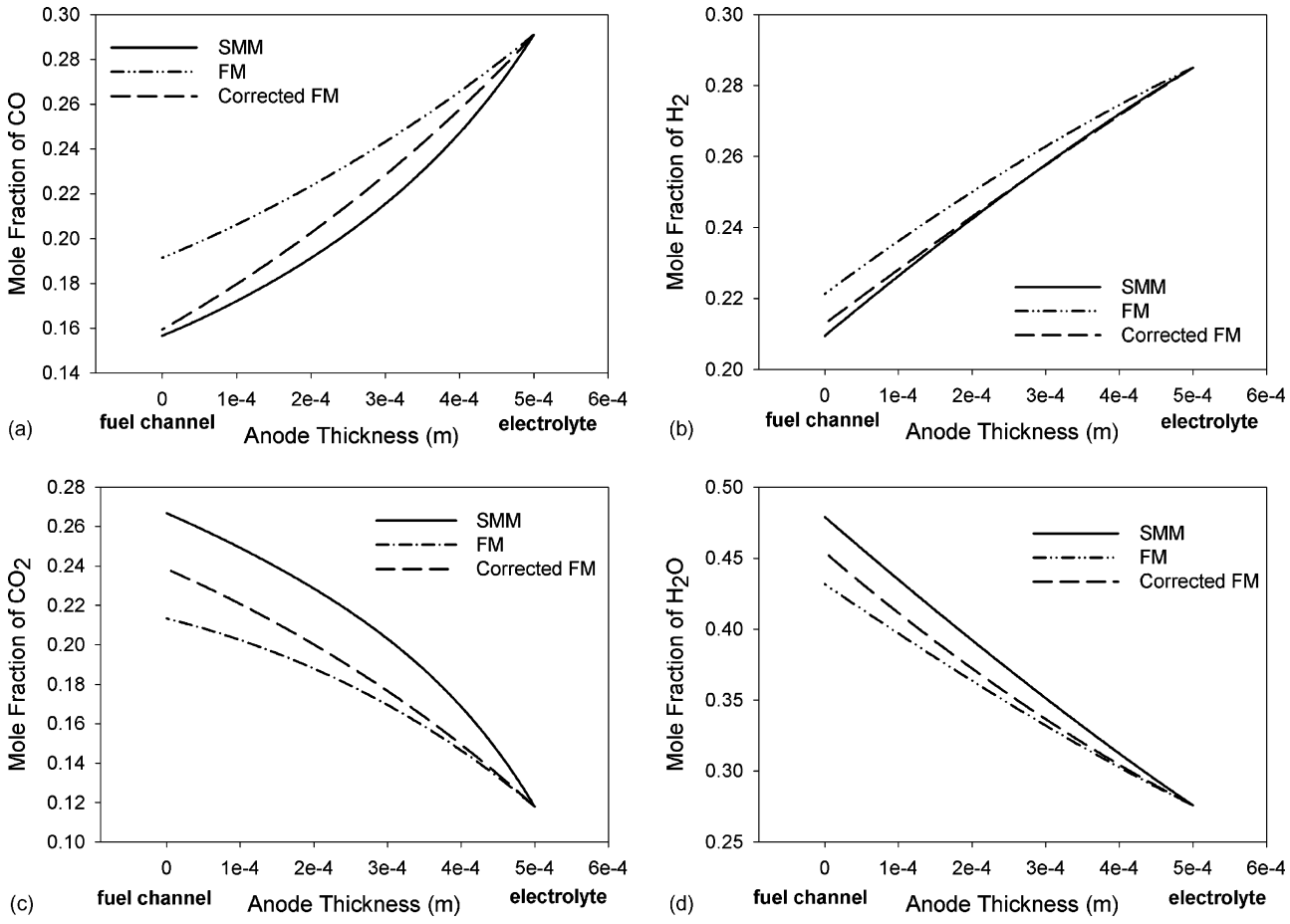

Fig. 5. Concentration profiles along the anode thickness predicted by FM and SMM for (a) CO, (b) H_2, (c) CO_2 and (d) H_2O at 4 A cm^{-2}.

Normalized reaction time scales (Table 4) indicate that, with the given inlet concentrations, steam methane reformation mostly proceeds in the forward direction whereas as water gas shift reactions may proceed in both directions. Moreover diffusion time scales are much smaller compared to reaction time scales indicating that this electrode is not limited by diffusion.

4. Application: button cell

In order to independently verify the proposed corrections to the effective diffusivities used in Fick's law type models applied to the multi-component mass transfer problems in fuel cells; this approach is employed in a three-dimensional simulation of a real button cell. The model used for these simulations is described elsewhere [18,19] in the literature and will not be covered here. The salient features of the model are that it allows for several species and bulk reactions on the anode side and it handles the simultaneous electrochemical oxidation on CO and H_2 without assuming a constant ratio between the current produced by each; rather this ratio is an outcome of the model (see Appendix). Also, the diffusion fluxes are calculated using Fick's law type relations and the effective diffusivities are calculated using the model in Eq. (10). The button cell simulated here is modeled after the experiments being performed at WVU [20]. The active area of the button cell is approximately 2 cm^2. The anode, electrolyte and cathode thicknesses are 780 μm, 20 μm and 200 μm respectively. The fuel stream fed to the anode has the composition shown in Table 5. The cathode side is supplied with air (21% O_2 and 79% N_2). Both air and fuel streams are supplied at a temperature of 800 °C. The flow field around the button cell is not included in the computation domain. However, its effect on the cell is taken into account using appropriate boundary conditions and transport properties. Given the low utilization of fuel and air in the button cell experiments, it was found that the current density distribution inside the cell was uniform at all currents.

Fig. 6 shows the experimentally measured and numerically computed VI curves for the button cell. Computations are performed both with and without the proposed correction to the effective multi-component diffusion coefficients. It can be seen from Fig. 6 that the agreement between the experiments and numerical predictions is good for low cell currents but at high currents the computations without correction to the diffusion coefficients fail to predict the onset of diffusion limitation of the cell performance.

Table 4
Normalized reaction time scales.

	τ_{chem}/τ_{conv}	
	Forward	Backward
Steam methane reforming	0.169621	1570.154
Water gas shift	0.069015	0.048962

Table 5
Fuel composition supplied to the anode.

Species	Mole fractions
H_2	0.303
CO	0.229
CO_2	0.209
H_2O	0.259

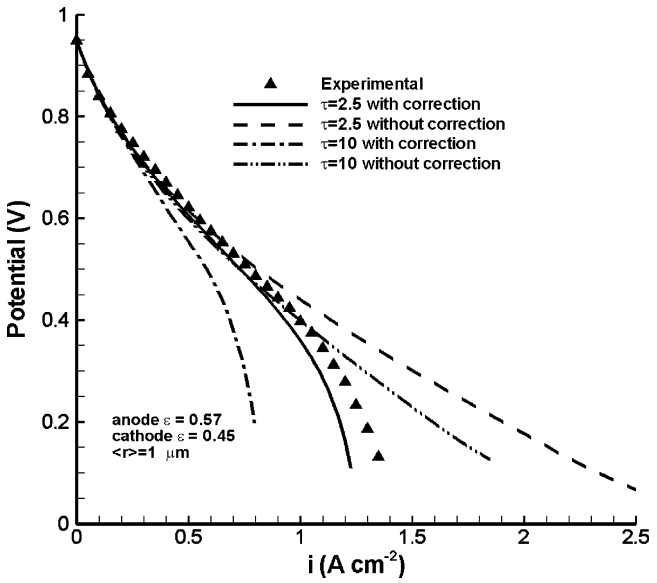

Fig. 6. Experimental and numerically simulated VI curves for the button cell.

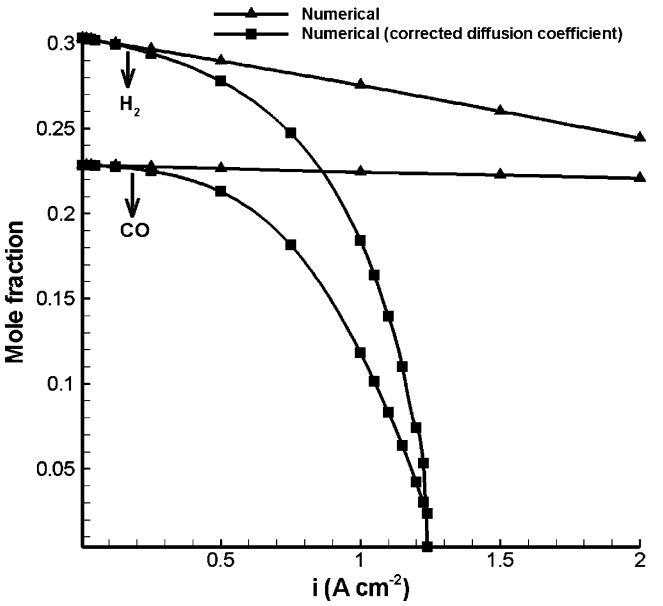

Fig. 7. Concentrations of H_2 and CO at the active anode/electrolyte interface as a function of cell current density.

However the numerical results with corrected diffusion coefficients accurately predict the limiting current though the agreement in terms of voltage values is poor near the limiting current region of the VI curve. It should be noted that a reasonable value of 2.5 [9,10] is used for tortuosity in these simulations. Though some researches [21,22] use higher values for tortuosity to calibrate diffusion limitation, they are not believed to be physically realistic [9,23]. For a thorough analysis, the simulations were repeated with a higher tortuosity of 10 with and without correction and the resulting VI curves are also plotted in Fig. 6. It can be seen that, although the voltages for $\tau = 10$ are lower than those for $\tau = 2.5$, the curve does not show the typical drop in voltage at high currents when no correction was applied. When the correction was applied with $\tau = 10$, the cell limiting current was found to be much lower than the experimentally observed value. It may thus be concluded that the inability of most numerical models to accurately predict the diffusion limitation is due to the inaccuracy resulting from Fick's law type diffusion model rather than the uncertainty in the tortuosity values. The limiting behavior is known to be due to the concentration of the reactants becoming very small near the active electrolyte/electrode interface.

In order to see how the concentrations of the H_2 and CO near the active interface are varying with the cell current, their mole fractions are plotted against the average cell current density in Fig. 7. Here it is seen that there is a huge difference in the prediction of interface concentrations obtained from simulations with and without the proposed correction, especially at high currents. The interface concentrations in the case of simulations without correction hardly change with cell current when compared to those with the correction. This is due to the reduction in diffusion coefficient as a function of current through the proposed correction. This could have significant effect on the concentration distributions and also chemical kinetics inside the anode. For example, the profiles of H_2 and CO mole fractions along the normalized thickness of the anode are shown in Figs. 8 and 9 respectively for the case of average cell current density 1 A cm^{-2}. Also the local production rate of H_2 (due to bulk reactions inside the anode) along the normalized thickness of anode for the same case is shown in Fig. 10. It can be seen that all these profiles are significantly different for cases with and without the correction. More interestingly, the production of H_2 is negative for the case without correction, indicating net consumption of hydrogen in the water gas shift reaction whereas it is positive for the case with correction. These differences are less prominent for cell currents lower than the case shown here and more prominent for higher cell current. These differences are to be expected since the concentrations and reaction rates are interdependent on each other and are sensitive to the diffusion coefficient which is widely different between these two cases, especially at high currents.

Fig. 11 shows the ratio of the current produced by H_2 to the current produced by CO oxidation as a function of cell current density. As was mentioned before this ratio is not assumed to be constant as done by some authors [17,24,25] but was determined as part of the solution. It can be seen from Fig. 11 that this ratio is in fact a function of the cell current density and as with the other variables, its value is affected by the proposed correction. With corrected diffusion, the proportion of current from CO oxidation seems to decrease with the cell current which is a result of nearly zero concentration of CO near the active interface at these currents as can be seen from Fig. 7. It should also be noted that in the simple mass transfer

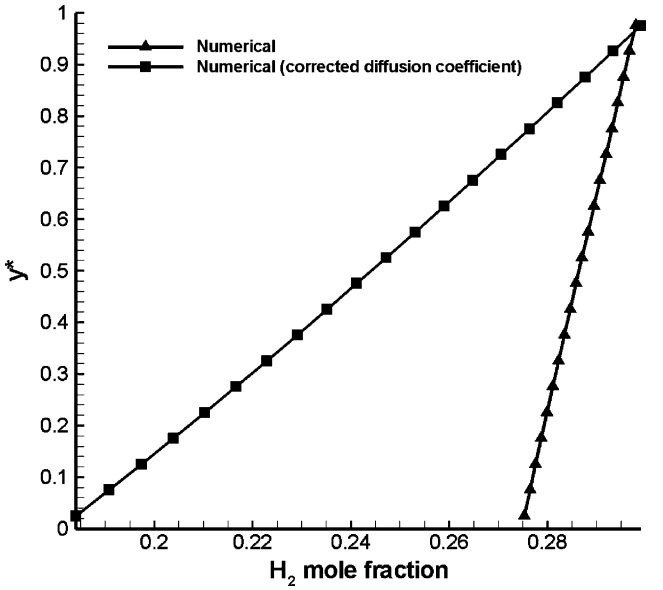

Fig. 8. Concentrations of H_2 along the normalized thickness of the anode for cell current density of 1 A cm^{-2}.

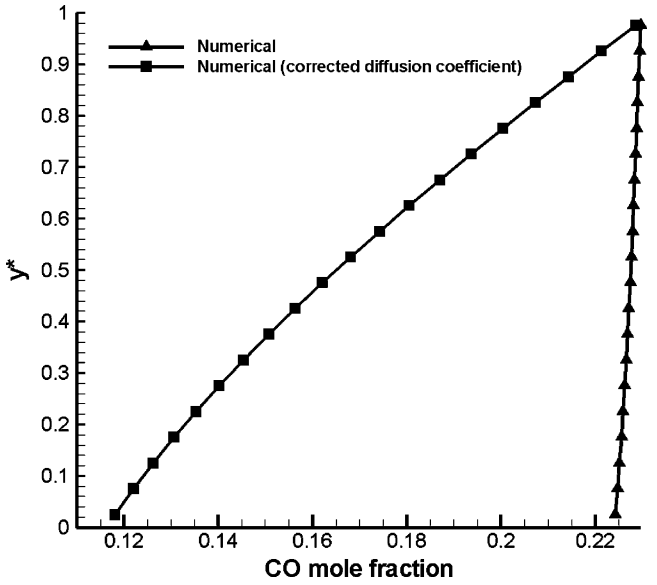

Fig. 9. Concentrations of CO along the normalized thickness of the anode for cell current density of 1 A cm^{-2}.

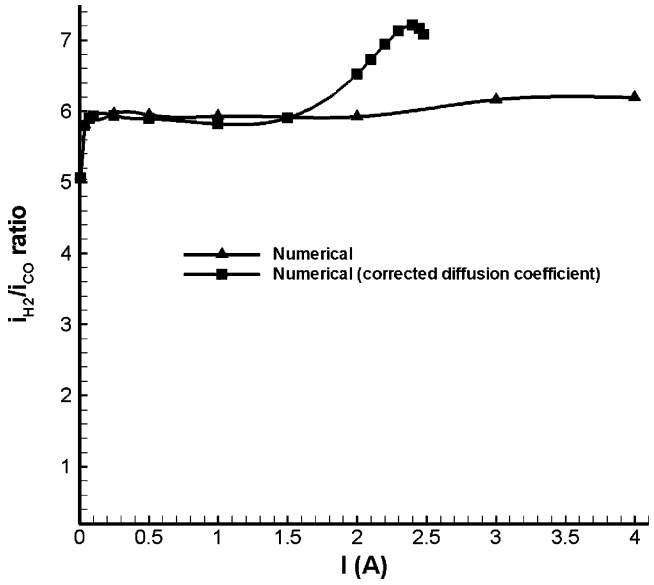

Fig. 11. Ratio between the current produced from H_2 oxidation and that from CO oxidation as a function of cell current.

calculations used to formulate the proposed correction, a constant ratio of 4 is assumed between H_2 and CO currents whereas this ratio seems to be getting as high as 7 when this correction is applied in a real cell. It remains to be tested if the correction is still valid under such conditions where this ratio is a function of cell current as well. This could be a possible reason for the disagreement between the voltage predictions using the corrected diffusion coefficient and the experiments shown in Fig. 6.

Finally, to investigate the effect of different fuel compositions on the limiting current, button cell simulations are repeated using $\tau = 2.5$ with corrected effected diffusivities and the results are shown in Fig. 12. The model results show expected dependence of VI curves on the fuel concentrations with voltages and limiting currents being higher when the concentration of fuel species (CO and H_2) is higher. Thus, it is shown that the proposed correction does not alter the response of the model to changes in fuel composition.

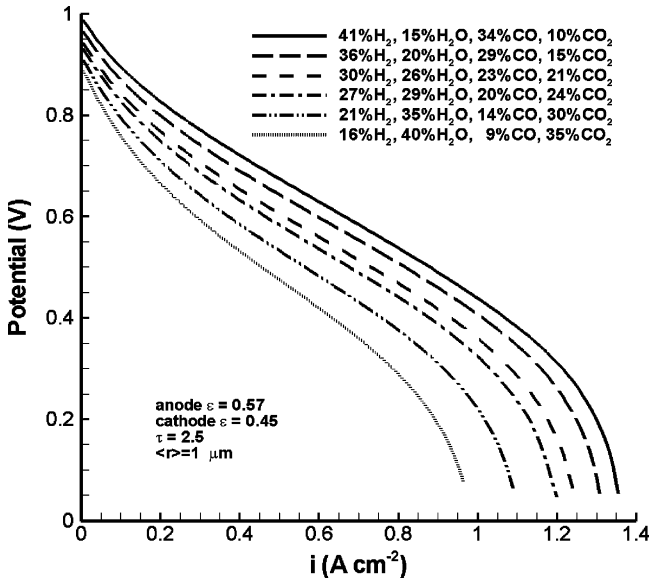

Fig. 12. Effect of fuel concentration on the VI curves.

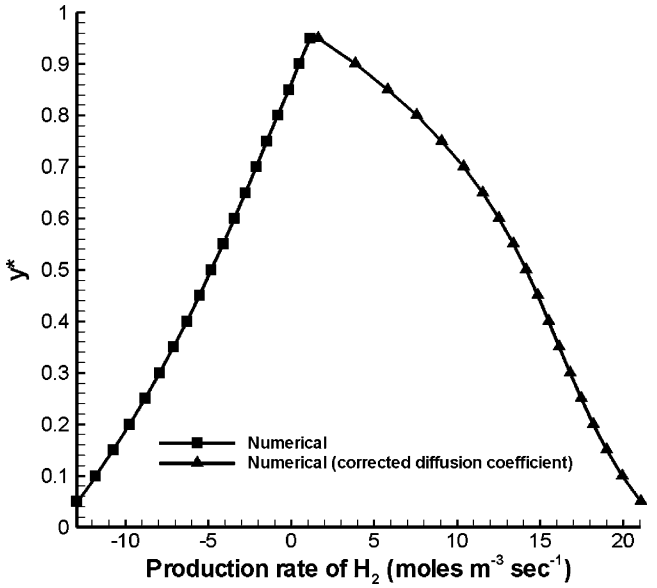

Fig. 10. Local production rate of H_2 along the thickness of the anode for cell current density of 1 A cm^{-2}.

5. Conclusions

Stefan–Maxwell model (SMM) and simple Fick's model (FM) type of relations both including Knudsen diffusion for the calculation of species mole fractions in a multi-component systems were compared and it was found that at low current densities the models agree well but as current increases the differences also increase. Based on the findings an empirical correction is proposed for the effective diffusivity used in Fick's model. The corrected diffusivity coefficient gave better agreement with the Stefan–Maxwell model and even at higher current densities the error is less than 5%. Proposed correction for effective diffusivity was applied to a three-dimensional, in-house SOFC simulation code which uses Fick's model type relations for diffusion flux calculations. As an application, an SOFC button cell which is being tested at West Virginia University was simulated. Numerical simulations with the corrected diffusivity accurately predicted the limiting current even with a reasonable tortuosity of 2.5. However, the predicted voltages

were slightly different from the experimental values near the limiting current region. Also the distributions of concentrations and reaction rates are widely different for the predictions with and without the proposed correction, especially at high current density. The ratio between the currents produced from H_2 and CO oxidation is a function of cell current density and is also affected by the correction.

Acknowledgements

This work is conducted under US DOE (Department of Energy) EPSCoR Program. It is jointly sponsored by US DOE Office of Basic Energy Sciences, NETL (National Energy Technology Laboratory), WV State EPSCoR Office and the West Virginia University under grant number DE-FG02-06ER46299. Dr. Tim Fitzsimmons is the DOE Technical Monitor. Dr. R. Bajura is the Administrative Manager and Dr. I. Celik is the Technical Manager and the Principal Investigator of this project.

The authors thank Dr. Chunchuan Xu and Dr. John Zondlo for providing the experimental data.

Appendix A

Electrochemistry model

The half cell reactions considered in the anode are

$$H_2 + O^{=} \rightarrow H_2O + 2e^{-} \quad \text{(A1)}$$

$$CO + O^{=} \rightarrow CO_2 + 2e^{-} \quad \text{(A2)}$$

and in the cathode the half cell reaction is

$$O_2 + 4e^{-} \rightarrow 2O^{=} \quad \text{(A3)}$$

Two overall reactions can be established as:

$$H_2 + 1/2O_2 \rightarrow H_2O \quad \text{(A4)}$$

$$CO + 1/2O_2 \rightarrow CO_2 \quad \text{(A5)}$$

The Nernst potential for reactions (A4) and (A5) is given respectively by

$$E_{H_2} = E^0_{H_2} - \frac{RT}{2F} \ln \left[\frac{P_{H_2O}}{P_{H_2} P^{0.5}_{O_2}} \right] \quad \text{(A6)}$$

$$E_{CO} = E^0_{CO} - \frac{RT}{2F} \ln \left[\frac{P_{CO_2}}{P_{CO} P^{0.5}_{O_2}} \right] \quad \text{(A7)}$$

Following the idea proposed by Nishino et al. [26] the potential across the electrolyte is given by

$$E_{H_2} - \eta_{H_2} - \eta_{O_2} = E_c - E_a \quad \text{(A8)}$$

$$E_{CO} - \eta_{CO} - \eta_{O_2} = E_c - E_a \quad \text{(A9)}$$

The calculation of the overpotentials (η_{H_2}, η_{CO} and η_{O_2}) is performed by using the Butler–Volmer equation:

$$i_s = i_{0,s} \left[\exp\left(\frac{\alpha n_s F}{RT} \eta_s \right) - \exp\left(-\frac{(1-\alpha) n_s F}{RT} \eta_s \right) \right] \quad \text{(A10)}$$

where the subscript s represents the species H_2, CO, and O_2.

Concentration overpotentials are not explicitly expressed in Eqs. (A8) and (A9) since partial pressures at the electrode–electrolyte interfaces are used in Eqs. (A6) and (A7). Similarly the ohmic overpotential is accounted for in the charge conservation equation.

In Eq. (A10) the charge transfer coefficient α is assumed as 0.5; n_s is the number of electrons transferred in the electrochemical reactions (A1)–(A3). The current densities i_{H_2} and i_{co} are the current densities driven by hydrogen and carbon monoxide respectively. $i_{O_2} = i_{tot}$ is the total current density given by

$$i_{tot} = i_{H_2} + i_{CO} \quad \text{(A11)}$$

Eqs. (A8)–(A11) form a set of equations to solve for hydrogen and carbon monoxide activation overpotentials and current densities.

References

[1] S.H. Chan, K.A. Khor, Z.T. Xia, Journal of Power Sources 93 (2001) 130–140.
[2] J.R. Ferguson, J.M. Fiard, R. Herbin, Journal of Power Sources 58 (1996) 109–122.
[3] H. Yakabe, M. Hishinuma, M. Uratani, Y. Matsuzaki, I. Yasuda, Journal of Power Sources 86 (2000).
[4] D. Sanchez, R. Chacartegui, A. Munoz, T. Sanchez, Journal of Power Sources 160 (2006) 1074–1087.
[5] R. Suwanwarangkul, E. Croiset, M.W. Fowler, P.L. Douglas, E. Entchev, M.A. Douglas, Journal of Power Sources 122 (2003) 9–18.
[6] J. Kim, A.V. Virkar, K. Fung, K. Mehta, S.C. Singhal, Journal of Electrochemical Society 146 (1999) 69–78.
[7] M. Ni, M.K.H. Leung, D.Y.C. Leung, Journal of Power Sources 163 (2006) 460–466.
[8] P. Leone, M. Santarelli, P. Asinari, M. Cali, R. Borchiellini, Journal of Power Sources 177 (2008) 111–122.
[9] R.E. Williford, L.A. Chick, G.D. Maupin, S.P. Simner, J.W. Stevenson, Journal of Electrochemical Society 150 (2003) A1067–A1072.
[10] J.R. Izzo, A.A. Peracchio, W.K.S. Chiu, Journal of Power Sources 176 (2008) 200–206.
[11] R. Krishna, J.A. Wesselingh, Chemical Engineering Science 52 (1997) 861–911.
[12] E.A. Mason, A.P. Malinauskas, Gas Transport in Porous Media: The Dusty Gas Model, Chemical Engineering Monographs, vol. 17, Elsevier, New York, 1983.
[13] E.L. Cussler, Diffusion Mass Transfer in Fluid Systems, 2nd ed., Cambridge University Press, Cambridge, UK, 1997.
[14] R.B. Bird, W.E. Stewart, E.N. Lightfoot, Transport Phenomena, 2nd ed., John Wiley & Sons, 2001.
[15] W. Lehnert, J. Meusinger, F. Thom, Journal of Power Sources 87 (2000) 57–63.
[16] B.A. Haberman, J.B. Young, International Journal of Heat and Mass Transfer 47 (2004) 3617–3629.
[17] R.S. Gemmen, J. Trembly, Journal of Power Sources 161 (2006) 1084–1095.
[18] S.R. Pakalapati, F. Elizalde-Blancas, I. Celik, Proceedings of Coal Based Fuel Cell Technology: Status, Needs and Future Applications, Morgantown, WV, October 11–12, 2007.
[19] F. Elizalde-Blancas, S.R. Pakalapati, J.A. Escobar-Vargas, I.B. Celik, Proceedings of 2008 ASME Fluids Engineering Division Summer Conference, Jacksonville, FL, 2008.
[20] J.W. Zondlo, C. Xu, Private Communication, 2008.
[21] Y. Jiang, A.V. Virkar, Journal of Electrochemical Society 150 (2003) A942–A951.
[22] A.V. Virkar, Low-temperature Anode-supported High Power Density Solid Oxide Fuel Cells with Nanostructured Electrodes, University of Utah, 2003.
[23] Y. Shi, N. Cai, C. Li, Journal of Power Sources 164 (2007) 639–648.
[24] Y. Matsuzaki, I. Yasuda, Journal of Electrochemical Society 147 (2000) 1630–1635.
[25] P. Aguiar, C.S. Adjiman, N.P. Brandon, Journal of Power Sources 138 (2004) 120–136.
[26] T. Nishino, H. Iwai, K. Suzuki, Journal of Fuel Cell Science and Technology 3 (2006) 33–44.